MATHEMATICAL MODELING AND COMPUTING, Vol. 10, No. 3, pp. 899–917 (2023)

Homogenization of the Helmholtz problem in the presence of a row of viscoelastic inclusions

Belemou R.[1], Sbitti A.[2], Jaouahri M.[1], Marigo J.-J.[3]

[1] *University Hassan II, Ens,*
El Jadida Km 9 Str., Ghandi, 50069, Casablanca, Maroc
[2] *University Mohammed V, Ensam,*
Nations Unies Str., Agdal, 8007 N.U., Rabat, Maroc
[3] *Solid Mechanics Laboratory, Ecole Polytechnique,*
91128, Palaiseau, France

(Received 15 April 2023; Revised 19 June 2023; Accepted 22 June 2023)

We propose a homogenization method based on a matched asymptotic expansion technique to obtain the effective behavior of a periodic array of linear viscoelastic inclusions embedded in a linear viscoelastic matrix. The problem is considered for shear waves and the wave equation in the harmonic regime is considered. The obtained effective behavior is that of an equivalent interface associated to jump conditions, for the displacement and the normal stress at the interface. The transmission coefficients and the displacement fields are obtained in closed forms and their validity is inspected by comparison with direct numerics in the case of a rectangular inclusions.

Keywords: *homogenization; matched asymptotic expansion; subwavelength scale; transmission of waves; viscoelastic; interface homogenization; effective jump conditions.*

2010 MSC: 74Q05 **DOI:** 10.23939/mmc2023.03.899

1. Introduction

The two-scale homogenization method is considered among the preferred tools for modeling wave propagation in periodic microstructures [1, 2]. However, classical homogenization methods are not efficient when considering media composed of micro-structured interfaces [3–5]: the behavior of the fields is dominated by boundary layer effects which are not taken into account by the theories of volume effective medium. To recover their efficiency, these methods must then be combined with matched asymptotic expansions, giving effective jump conditions on an equivalent interface. These methods have been used in static elasticity [6, 7]. For the propagation of waves, they have been adapted in elasticity, studies have focused on rows of non-resonant inclusions [8,9] then on resonant inclusions [10]. For the propagation of waves in electromagnetism [11–13], and in acoustics [5, 14]. We also note that similar methods can also be used to obtain effective jump conditions for stratified media [15–17], metallic structures [18, 19], adhesive layers [20–22], bubble screens [9], Helmholtz resonators [23, 24] and for the latter, the results are equivalent to those obtained with the energy-based methods [25–27]. The case of non-periodic layers has also been studied for seismic waves [28].

In this article, we used the asymptotic analysis and the same homogenization approach that was applied in the case of shear wave scattering by a periodic row of elastic inclusions embedded in elastic matrix [8, 10]. We have noticed that in the case of viscoelastic linear media, the wave equation of the real problem in the harmonic regime takes the same form as that in elasticity, except that in our case the coefficients of the physical parameters entering the equation are complex, which does not change the homogenization procedure and even the form of the homogenized wave equations obtained at different orders. We also show that the diffusion parameters of the effective model accurately describe those of the real structure, and in general, the homogenized solution associated with the jump condition is even more meaningful than the classical homogenization.

The paper is organized as follows. In Section 2, we summarize the result of the asymptotic analysis in the case of a row of linear viscoelastic inclusions inserted periodically in a linear viscoelastic matrix, the main derivation steps of which are given in the Appendix Ann.4. The resulting system (7) represents the homogenized problem associated with the jump conditions of displacement and normal stress through an equivalent interface. In Section 3, the accuracy of the actual model is verified by comparison with numerical values based on the multimodal method [17] for an incident shear wave. Transmission coefficients as a function of frequency $K_R h$, inclusion thickness e/h and as a function of reciprocal quality factor Q^{-1} are illustrated and the agreement between real and actual problems is discussed.

2. The real problem and the effective problem

We summarize below the main results of the asymptotic analysis in Appendix Ann.4, and which provides the so-called "effective problem" where the row of linear viscoelastic inclusions is replaced by an equivalent interface associated with jump conditions for displacement and normal stress (Figure 1).

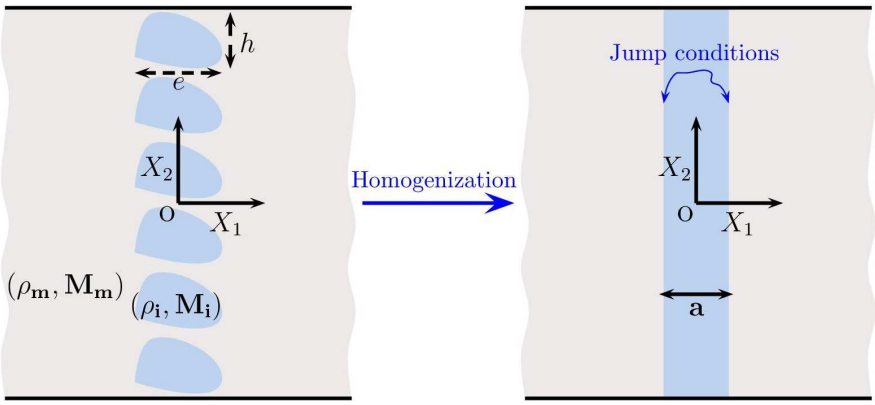

Fig. 1. A row of inclusions in the matrix of thickness e and width h, are replaced by a layer of thickness a through which the jump conditions are applied.

2.1. The physical problem

We consider the shear wave propagating in a viscoelastic matrix Ω_m containing a row of periodically located viscoelastic inclusions, $(\Omega_r = \cup\Omega_i,\ i = 1, 2, \ldots, N_r)$ with spacing h and thickness $e = O(h)$ of each inclusion Ω_i (Figure 1). The scalar displacement field $U(\mathbf{X})$ written in the harmonic regime wave case, with $\mathbf{X} \in \Omega$ the spatial coordinates $(\Omega = \Omega_m \cup \Omega_r)$ and $\Omega = \{(X_1, X_2) \in \mathbb{R} \times (-H/2, H/2)\}$.

$$\operatorname{div}(M\boldsymbol{\nabla} U) + \rho\omega^2 U = 0, \tag{1}$$

with M and ρ being respectively the complex shear modulus and the mass density, and ω the frequency. The equation (1) can be written using the dimensionless parameters.

$$\alpha^*(\mathbf{X}) \equiv \frac{M(\mathbf{X}, \omega)}{M_m} \quad \text{and} \quad \beta(\mathbf{X}) \equiv \frac{\rho(\mathbf{X})}{\rho_m},$$

with M_m the complex shear modulus and ρ_m the mass density of the viscoelastic matrix occupying the Ω/Ω_r region; with $K^* = \omega\sqrt{\rho_m/M_m}$ the complex wave number in the matrix, we obtain:

$$\operatorname{div}(\alpha^* \nabla U) + \beta K^{*2} U = 0, \tag{2}$$

allowing us to write the Helmholtz equation in the matrix as follows:

$$\Delta U + K^{*2} U = 0.$$

In the harmonic regime, we consider viscoelastic waves with a wavelength $2\pi/K_R$ very large compared to the periodicity of the inclusions h (K_R being the real part of the complex shear wave num-

ber K^*), such that:

$$\varepsilon = K_R h \ll 1.$$

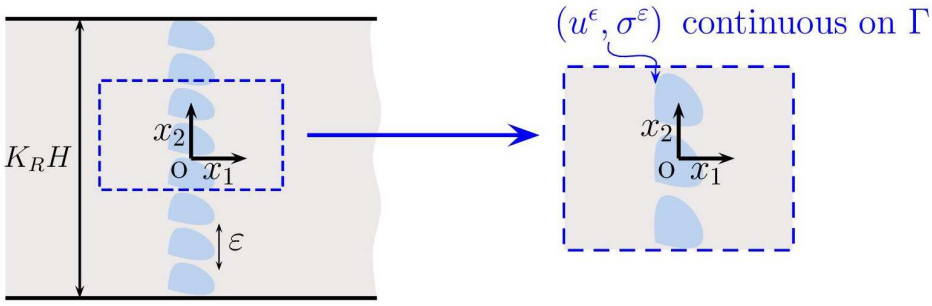

Fig. 2. Real problem in adimensional coordinates with ($x_1 = K_R X_1$, $x_2 = K_R X_2$). The usual continuity conditions for $(u^\varepsilon, \sigma_2^\varepsilon)$ apply to the Γ boundaries between the inclusions and the substrate.

To be consistent, we will work in dimensionless coordinates with ($x_1 = K_R X_1$, $x_2 = K_R X_2$). We consider the real problem for $\mathbf{x} = (x_1, x_2) \in \mathbb{R} \times (-K_R H/2, K_R H/2)$ (Figure 2). We note

$$a^{*\varepsilon}(\mathbf{x}) \equiv \alpha^*(\mathbf{X}), \quad b^{*\varepsilon}(\mathbf{x}) \equiv \beta(\mathbf{X}) \left(\frac{K^*}{K_R}\right)^2;$$

$$u^\varepsilon(\mathbf{x}) \equiv U(\mathbf{X}), \quad \sigma^\varepsilon(\mathbf{x}) \equiv {K_R}^{-1} \alpha^*(\mathbf{X}) \nabla U(\mathbf{X}),$$

where the functions a^* and b^* are 1-periodic and complex, such that:

$$a^{*\varepsilon}(\mathbf{x}) = a^*\left(\frac{x_2}{\varepsilon}\right) \quad \text{and} \quad b^{*\varepsilon}(\mathbf{x}) = b^*\left(\frac{x_2}{\varepsilon}\right). \tag{3}$$

Moreover, we have explicitly stated the dependence of $(u^\varepsilon, \sigma^\varepsilon)$ on ε, being the periodicity of inclusions in dimensionless form. Now (2) reads:

$$\begin{cases} \operatorname{div} \sigma^\varepsilon(\mathbf{x}) + b^{*\varepsilon}(\mathbf{x}) u^\varepsilon(\mathbf{x}) = 0, & \mathbf{x} \in \Omega; \\ \sigma^\varepsilon(\mathbf{x}) = a^{*\varepsilon}(\mathbf{x}) \nabla u^\varepsilon(\mathbf{x}); \\ u^\varepsilon \text{ and } \sigma^\varepsilon \cdot \mathbf{n} \text{ continuous} & \mathbf{x} \in \partial\Omega_i, \quad i = 1, 2, \ldots, N_r, \end{cases} \tag{4}$$

where in this case, the functions a^* and b^* are 1-periodic and piecewise complex constant, such that:

$$a^{*\varepsilon}(\mathbf{x}) = \begin{cases} 1, & \Omega/\Omega_r, \\ a^*\left(\frac{x_2}{\varepsilon}\right), & \Omega_r; \end{cases} \qquad b^{*\varepsilon}(\mathbf{x}) = \begin{cases} \left(\frac{K^*}{K_R}\right)^2, & \Omega/\Omega_r, \\ b^*\left(\frac{x_2}{\varepsilon}\right), & \Omega_r. \end{cases} \tag{5}$$

The boundary conditions at $|x_1| \to +\infty$ and $x_2 = \pm K_R H/2$, are called radiation conditions, apply once the wave source has been defined. For the moment, we do not need to specify their form.

2.2. Effective interface and classical effective medium models

In the effective interface model [8], this is done by imposing the jump conditions between $x = -e/2$ and $x = e/2$. In the classical effective mean model [29], this is done by replacing the row of inclusions by a homogeneous and anisotropic slab. Both models are based on an asymptotic method and are valid in the limit $kh \ll 1$, we will see the predictions hold up to $kh \sim 1$ with reasonable errors.

2.2.1. Effective interface model

The homogenized problem of the real problem (4), is done by defining the fields (u^h, σ^h) satisfying the Helmholtz equation in the matrix and the associated jump conditions (see Ann.4), and is written as

follows:

$$\begin{cases} \Delta u^h + u^h = 0, \\ [\![u^h]\!] = \varepsilon \mathcal{B} \overline{\dfrac{\partial u^h}{\partial x_1}} + \varepsilon B_2 \overline{\dfrac{\partial u^h}{\partial x_2}}, \\ [\![\sigma_1^h]\!] = \varepsilon \left[\mathcal{S} \overline{\operatorname{div} \sigma^h} - \mathcal{C}_1 \overline{\dfrac{\partial {\sigma_1}^h}{\partial x_2}} - \mathcal{C} \overline{\dfrac{\partial {\sigma_2}^h}{\partial x_2}} \right], \end{cases} \tag{6}$$

where the jump conditions and associated mean value for any field are defined as follows:

$$[\![f]\!] \equiv f^+ - f^-, \quad \bar{f} \equiv \frac{1}{2}\left[f^- + f^+\right],$$

with

$$f^{\pm} = f\left(\pm \frac{eK_R}{2}, x_2\right),$$

and

$$\mathcal{B} \equiv \frac{e}{h} + \mathcal{B}_1, \quad \mathcal{C} \equiv \frac{e}{h} + \frac{e\varphi}{h}\left(\frac{M_i}{M_m} - 1\right) + \mathcal{C}_2, \quad S \equiv \frac{e}{h} + \frac{e\varphi}{h}\left(\frac{\rho_i}{\rho_m} - 1\right),$$

with $(\mathcal{B}_i, \mathcal{C}_i, i = 1, 2)$ the interface parameters (32)–(43), and φ is the filling fraction of each inclusion in the row. M_i is the complex shear modulus and ρ_i is the mass density of the viscoelastic inclusions occupying the Ω_r region.

Finally, from (6) and return to real space to obtain the final homogenized problem, which will be defined outside the interface occupying $\mathbf{X} \in (-e/2, e/2) \times (-\infty, +\infty)$, and is written as follows:

$$\begin{cases} \Delta U^h + {K^*}^2 U^h = 0, \quad |X_1| > \dfrac{e}{2}, \\ [\![U^h]\!]_e = h\mathcal{B} \overline{\dfrac{\partial U^h}{\partial x_1}} + hB_2 \overline{\dfrac{\partial U^h}{\partial x_2}}, \\ [\![\Sigma_1^h]\!]_e = h \left[\mathcal{S} \overline{\operatorname{div} \Sigma^h} - \mathcal{C}_1 \overline{\dfrac{\partial {\Sigma_1}^h}{\partial x_2}} - \mathcal{C} \overline{\dfrac{\partial {\Sigma_2}^h}{\partial x_2}} \right], \end{cases} \tag{7}$$

with $[\![F]\!] \equiv F(e/2, X_2) - F(-e/2, X_2)$ and $\overline{F} \equiv 1/2\,[F(e/2, X_2) + F(-e/2, X_2)]$.

2.2.2. Classic effective medium model

Classical homogenization tells us that a medium composed of inclusions can be replaced by an equivalent homogeneous and anisotropic medium described by the wave equation, as follows:

$$\begin{cases} \operatorname{div}\left(\begin{pmatrix} \langle a^* \rangle & 0 \\ 0 & \langle 1/a^* \rangle^{-1} \end{pmatrix} \nabla U^h \right) + \langle b^* \rangle {K_R}^2 U^h = 0, & |X_1| < \dfrac{e}{2}, \\ \Delta U^h + {K^*}^2 U^h = 0, & |X_1| > \dfrac{e}{2}, \\ U^h \text{ and } \Sigma^h \cdot \mathbf{n} \text{ continuous} & X_1 = -e/2, e/2, \end{cases} \tag{8}$$

involving effective parameters $\left(\langle a^* \rangle, \langle 1/a^* \rangle^{-1}\right)$ and $\langle b^* \rangle$ defined by:

$$\begin{cases} \langle a^* \rangle = \varphi \dfrac{M_i}{M_m} + 1 - \varphi, & \langle 1/a^* \rangle^{-1} = \left[\varphi \dfrac{M_m}{M_i} + 1 - \varphi \right]^{-1}, \\ \langle b^* \rangle = \left(\dfrac{K^*}{K_R} \right)^2 \left(\varphi \dfrac{\rho_i}{\rho_m} + 1 - \varphi \right). \end{cases} \tag{9}$$

3. Numerical validation of the actual problem

In this section, we discuss the error of the homogenized solution with respect to the solution of the real problem, we consider the particular diffusion problem of a row of square, or rectangular inclusions. Note that for rectangular inclusions, being symmetric about y_2, $V^{(1)}$ is symmetric and $V^{(2)}$ is anti-symmetric about y_2; it follows that $\mathcal{B}_2 = \mathcal{C}_1 = 0$ in (32) and (43), and only ($\mathcal{S}$, $\mathcal{B}$, $\mathcal{C}$) are needed in the jump conditions. These effective parameters are determined numerically by using a multi-modals method (see [8]).

3.1. Solutions of the physical problem

We numerically solve the real problem of an incident shear wave of type SII [30], which coming from $X_1 < -e/2$ and hitting the inclusion row at oblique incidence θ with heterogeneity degree γ (Figure 3). To do this, the multimodal method is used (see [31]).

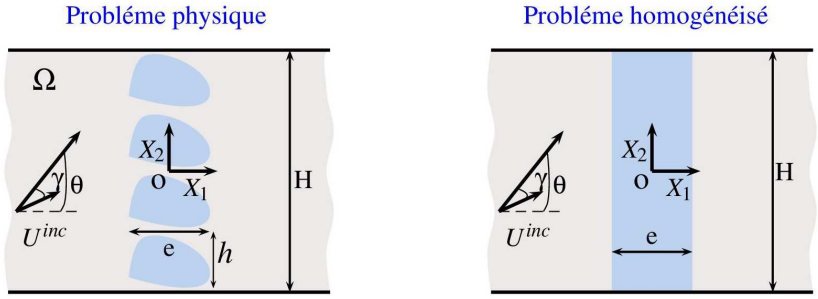

Fig. 3. Left: Real problem of plane wave scattering at oblique incidence θ by a row of rectangular voids, with a degree of heterogeneity γ. Right: The homogenized problem involves an interface of equal thickness e, which is associated with jump conditions applying to $X_1 = \pm e/2$.

We will work with complex fields (because the physical fields are the real parts of the calculated complex fields); in the harmonic regime, the complex fields (and we will consider the displacement field $U(X)$) have a time dependence in $e^{-\mathrm{i}\omega t}$ and it will be omitted in the following. This type of shear wave is defined as a SII type wave [30], of the following form:

$$U^{\mathrm{inc}}(\mathbf{X}) = e^{-\mathrm{i}\omega t} e^{i\boldsymbol{K}\cdot\boldsymbol{r}} = e^{-\mathrm{i}\omega t} e^{-\boldsymbol{A}\cdot\boldsymbol{r}} e^{i\boldsymbol{P}\cdot\boldsymbol{r}}, \tag{10}$$

where $\boldsymbol{r} = (X_1, X_2)$ is the position vector, and $\boldsymbol{K}$ the complex wave vector is given by

$$\boldsymbol{K} = \boldsymbol{P} + i\boldsymbol{A} = K_S \hat{x_1} + K_{inc} \hat{x_2}$$

and the corresponding propagation and attenuation vectors, are given by

$$\boldsymbol{P} = |\boldsymbol{P}| \cos(\theta)\hat{x_2} + |\boldsymbol{P}| \sin(\theta)\hat{x_2} = \mathrm{Re}[K_S]\hat{x_1} + \mathrm{Re}[K_{\mathrm{inc}}]\hat{x_2},$$
$$\boldsymbol{A} = |\boldsymbol{A}| \cos(\theta - \gamma)\hat{x_1} + |\boldsymbol{A}| \sin(\theta - \gamma)\hat{x_2} = \mathrm{Im}[K_S]\hat{x_1} + \mathrm{Im}[K_{\mathrm{inc}}]\hat{x_2},$$

with $(\hat{x_1}, \hat{x_2})$ are orthogonal real unit vectors for a Cartesian coordinate system, k_{inc} is the complex wave number for the assumed general SII wave, and $K_S = \sqrt{K^{*2} - {K_{\mathrm{inc}}}^2}$, where "$\sqrt{\ }$" is understood to indicate the principal value of the square root of a complex number $z = z_R + \mathrm{i}\, z_I$ defined in terms of the positive square root of real numbers by

$$\sqrt{z} = \sqrt{\frac{|z| + z_R}{2}} + \mathrm{i}\,\mathrm{sign}[z_I]\sqrt{\frac{|z| - z_R}{2}}$$

with

$$\mathrm{sign}[z_I] \equiv \left\{ \begin{array}{ccc} 1 & \text{if} & z_I \geqslant 0 \\ -1 & \text{if} & z_I < 0 \end{array} \right\}$$

hence, the complex wave numbers K_{inc} and K_S reads

$$K_{\mathrm{inc}} = |\boldsymbol{P}| \sin(\theta) + \mathrm{i}|\boldsymbol{A}| \sin(\theta - \gamma),$$
$$K_S = |\boldsymbol{P}| \cos(\theta) + \mathrm{i}|\boldsymbol{A}| \cos(\theta - \gamma),$$

where the magnitudes of the propagation and attenuation are specified in terms of the given material parameters, the complex wave number K^* or wave speed ($v_m = \omega/K_R$) and the reciprocal quality factors (${Q_m}^{-1} = M_{mI}/M_{mR}$), and the given degree of inhomogeneity γ [30].

The reference numerical solution U^{num} is searched in the matrix where the Helmholtz equation applies and U and $\Sigma \cdot \mathbf{n}$ being continuous at each interface between the matrix and the inclusion. The current problem is placed in Ω_m being the region occupied by the matrix and we denote $\Omega_r = \cup\Omega_i$, $(i = 1, 2, \ldots, N_r)$ the row occupied by each inclusion Ω_i, with $K_i^* = \omega\sqrt{\rho_i/M_i}$ the complex wavenumber in the inclusions,

$$\begin{cases} \Delta U + K^{*2}U = 0, & X \in \Omega_m, \\ \Delta U + {K_i}^{*2}U = 0, & X \in \Omega_i,\ i = 1, 2, \ldots, N_r, \\ U \text{ and } \Sigma \cdot \mathbf{n} \text{ continuous on} & X_1 \in \partial\Omega_i,\ i = 1, 2, \ldots, N_r, \\ \lim\limits_{X \to \pm\infty} \left[\dfrac{\partial}{\partial X_1} \left(U - U^{\text{inc}}\right) \pm iK_S \left(U - U^{inc}\right) \right] = 0, & \\ U\left(X_1, \dfrac{H}{2}\right) = e^{\mathrm{i}K_{\text{inc}}} U\left(X_1, -\dfrac{H}{2}\right), & X_1 \in \mathbb{R}, \\ \dfrac{\partial U}{\partial X_2}\left(X_1, \dfrac{H}{2}\right) = e^{\mathrm{i}K_{\text{inc}}} \dfrac{\partial U}{\partial X_2}\left(X_1, -\dfrac{H}{2}\right), & X_1 \in \mathbb{R}, \end{cases} \tag{11}$$

where the scattered waves $(U - U^{\text{inc}})$ at $X_1 \to \pm\infty$ satisfy the radiation condition [32], and are considered in the low frequency regime [5]. The last condition represents the pseudo-periodicity [33], which applies in the case where $H = nh$, with n an integer, for the incident wave and for the total field.

3.2. Homogenized problem solutions

We will check the accuracy of the homogenized solution of the effective interface problem (12) and the classical effective model (8). To do this, we treat two particular problems of diffusion by a row of rectangular inclusions. Thus, the matrix is considered a linear viscoelastic medium with a reciprocal quality factor Q_m^{-1}, which is different from the reciprocal quality factor Q_{in}^{-1} of linear viscoelastic inclusions.

3.2.1. Solutions of the effective interface model

Solutions of the effective interface model (7) with (10) is of the form:

$$\begin{cases} \Delta U^h + K^{*2}U^h = 0, & |X_1| > \dfrac{e}{2}, \\ [\![U^h]\!]_e = h\mathcal{B}\overline{\dfrac{\partial U^h}{\partial x_1}}, & \\ [\![\Sigma_1^h]\!]_e = h\left[\mathcal{S}\overline{\operatorname{div}\Sigma^h} - \mathcal{C}\overline{\dfrac{\partial {\Sigma_2}^h}{\partial x_2}}\right], & \\ \lim\limits_{X_1 \to \pm\infty} \left[\dfrac{\partial}{\partial X_1} \left(U^h - U^{\text{inc}}\right) \mp \mathrm{i}K_S \left(U^h - U^{\text{inc}}\right) \right] = 0, & \\ U^h\left(X_1, \dfrac{H}{2}\right) = e^{\mathrm{i}K_{\text{inc}}} U^h\left(X_1, -\dfrac{H}{2}\right), & X_1 \in \mathbb{R} \\ \dfrac{\partial U^h}{\partial X_2}\left(X_1, \dfrac{H}{2}\right) = e^{\mathrm{i}K_{\text{inc}}} \dfrac{\partial U^h}{\partial X_2}\left(X_1, -\dfrac{H}{2}\right), & X_1 \in \mathbb{R} \end{cases} \tag{12}$$

The solution of (12) is written

$$\begin{cases} U(\mathbf{X}) = \left[e^{\mathrm{i}K_S(X_1 + e/2)} + \mathbf{R}e^{-\mathrm{i}K_S(X_1+e/2)}\right] e^{\mathrm{i}K_{inc}X_2}, & X_1 < -e/2, \\ U(\mathbf{X}) = \left[\mathbf{T}e^{\mathrm{i}K_S(X_1 - e/2)}\right] e^{\mathrm{i}K_{\text{inc}}X_2}, & X_1 > e/2, \end{cases} \tag{13}$$

with (R,T) are given using jump conditions (12) with (13). The transmission coefficient T and reflection coefficient R is read:

$$\begin{cases} R = \dfrac{1}{2}\left[\dfrac{z_4^*}{z_3} - \dfrac{z_2^*}{z_1}\right], \\ T = \dfrac{1}{2}\left[\dfrac{z_4^*}{z_3} + \dfrac{z_2^*}{z_1}\right], \end{cases} \tag{14}$$

with

$$\begin{cases} z_1 \equiv 1 - \mathrm{i}\dfrac{h}{2}\mathcal{B}K_S, \\ z_1 \equiv 1 + \mathrm{i}\dfrac{h}{2}\mathcal{B}K_S, \\ z_2 \equiv K_S - \mathrm{i}\dfrac{h}{2}\left(\mathcal{S}\left(K_S^2 + K_{\mathrm{inc}}^2\right) - \mathcal{C}K_{\mathrm{inc}}^2\right), \\ z_2 \equiv K_S + \mathrm{i}\dfrac{h}{2}\left(\mathcal{S}\left(K_S^2 + K_{\mathrm{inc}}^2\right) - \mathcal{C}K_{\mathrm{inc}}^2\right). \end{cases} \tag{15}$$

3.2.2. Solutions of the classical effective medium

The homogenized classical problem (8) with the incident (10) takes the following form:

$$\begin{cases} \operatorname{div}\left(\begin{pmatrix} \langle a^*\rangle & 0 \\ 0 & \langle 1/a^*\rangle^{-1} \end{pmatrix}\nabla U^h\right) + \langle b^*\rangle {K_R}^2 U^h = 0, & |X_1| < \dfrac{e}{2}, \\ \Delta U^h + {K^*}^2 U^h = 0, & |X_1| > \dfrac{e}{2}, \\ U^h \text{ and } \Sigma^h \cdot \mathbf{n} \text{ continuous on} & X_1 = -e/2, e/2, \\ \lim\limits_{X_1 \to \pm\infty}\left[\dfrac{\partial}{\partial X_1}\left(U^h - U^{\mathrm{inc}}\right) \mp \mathrm{i}K_S\left(U^h - U^{\mathrm{inc}}\right)\right] = 0, & \\ U^h\left(X_1, \dfrac{H}{2}\right) = e^{\mathrm{i}K_{\mathrm{inc}}} U^h\left(X_1, -\dfrac{H}{2}\right), & X_1 \in \mathbb{R}, \\ \dfrac{\partial U^h}{\partial X_2}\left(X_1, \dfrac{H}{2}\right) = e^{\mathrm{i}K_{\mathrm{inc}}} \dfrac{\partial U^h}{\partial X_2}\left(X_1, -\dfrac{H}{2}\right), & X_1 \in \mathbb{R}. \end{cases} \tag{16}$$

The solution of (16) is written:

$$\begin{cases} U(\mathbf{X}) = \left[e^{\mathrm{i}K_S(X_1 + e/2)} + \mathbf{R}e^{-\mathrm{i}K_S(X_1+e/2)}\right] e^{\mathrm{i}K_{\mathrm{inc}}X_2}, & X_1 < -\dfrac{e}{2}, \\ U(\mathbf{X}) = \left[ae^{\mathrm{i}KX_1} + be^{-\mathrm{i}KX_1}\right] e^{\mathrm{i}K_{\mathrm{inc}}X_2}, & |X_1| < \dfrac{e}{2}, \\ U(\mathbf{X}) = \mathbf{T}e^{\mathrm{i}K_S(X_1 - e/2) + \mathrm{i}K_{\mathrm{inc}}X_2}, & X_1 > \dfrac{e}{2}, \end{cases} \tag{17}$$

on $X_1 = -e/2, e/2$, using the continuities of U^h and $\Sigma_h \cdot \mathbf{n}$, we obtain the diffusion coefficients (R,T) of the form

$$\begin{cases} R = \dfrac{2i\left(K_S^2 - K^2\xi^2\right)\sin Ke}{(K_S - K\xi)^2 e^{\mathrm{i}Ke} - (K_S + K\xi)^2 e^{-\mathrm{i}Ke}}, \\ T = -\dfrac{4KK_S\xi}{(K_S - K\xi)^2 e^{\mathrm{i}Ke} - (K_S + K\xi)^2 e^{-\mathrm{i}Ke}}, \end{cases} \tag{18}$$

with

$$K = \sqrt{\frac{\langle b^*\rangle}{\langle a^*\rangle}K_R^2 - \frac{\langle 1/a^*\rangle^{-1}}{\langle a^*\rangle}K_{\mathrm{inc}}^2}, \quad \xi = \phi\frac{M_i}{M_m} + 1 - \phi.$$

3.3. Accuracy of the homogenized solution compared to the real solution

We will check the validity of the homogenized solution for an oblique incident wave. We first introduce the fields U^{num} numerically calculated (11) and the U^h fields of classical homogenized solutions (8) and interface (13), this is done for low-loss viscoelastic media $Q^{-1} \ll 1$ and for no Low-loss media $Q^{-1} \geqslant 0.2$) (Figure 4). We will also present numerical and homogenized solutions for the case of ($Q^{-1} \geqslant 0.2$), but this time varying e/h the geometric shape of the inclusions (Figure 5).

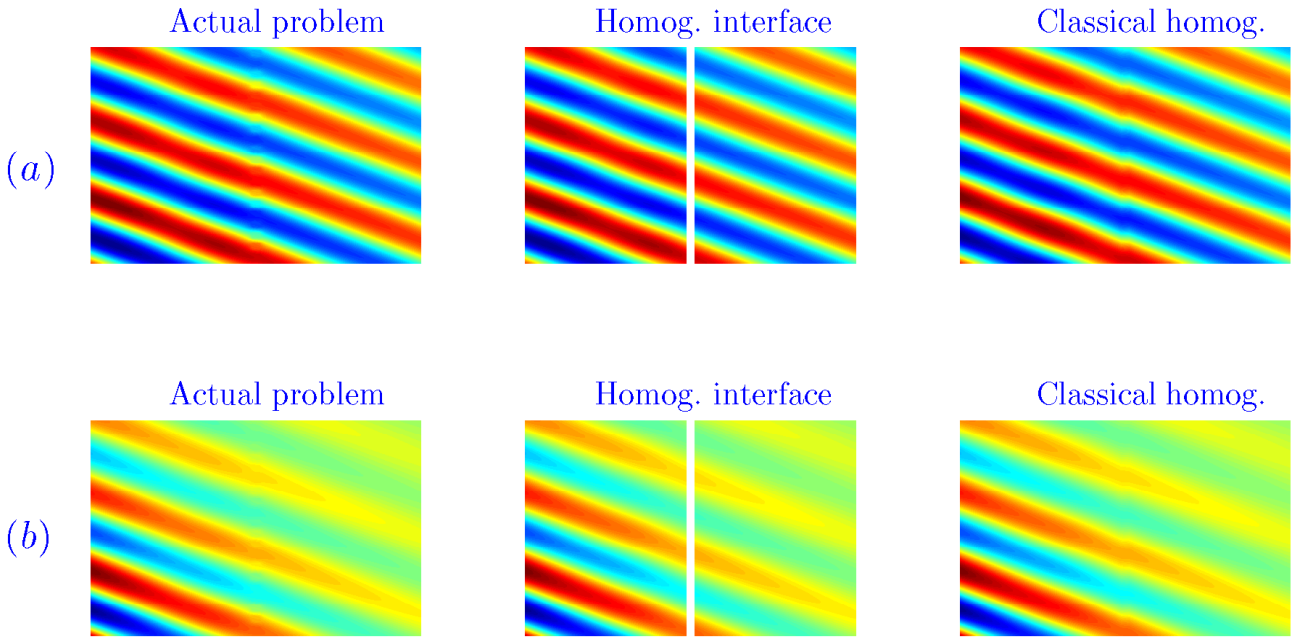

Fig. 4. (a) The numerical solution U^{num} in the real problem of low-loss viscoelastic media $Q_m^{-1} = 0.05$ and $Q_{in}^{-1} = 0.1$, for an oblique incident plane wave $\theta = \pi/3$ with a degree of heterogeneity $\gamma = \pi/6$ and $K_R h = 1$. Reflected by a slab of rectangular voids ($h = 1$, $e/h = 0.5$ and $\varphi = 0.5$); (b) Same representation as (a) with $Q_m^{-1} = 0.2$ and $Q_{in}^{-1} = 0.3$ in the case of viscoelastic media (no low-loss media).

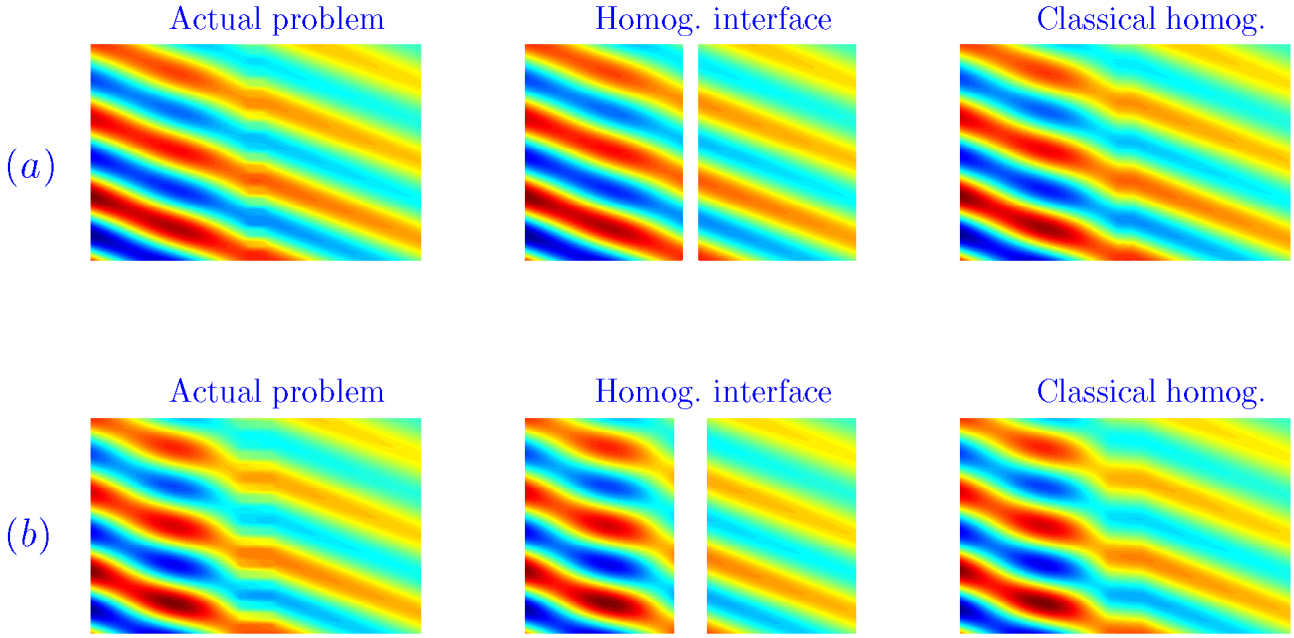

Fig. 5. (a) Same representation as (Figure 4) with the reciprocal quality factor $Q_m^{-1} = 0.1$ and $Q_{in}^{-1} = 0.2$. (b) Same representation as (a) with $e/h = 1$.

Defining $\Delta U \equiv |U - U^{\text{num}}|/|U^{\text{num}}|$ (for $|X_1| > e/2$ with $\|\cdot\|$ the norm L^2), we obtain, on average, the results indicated in the table (Table 1). It is interesting to note that a small error was found even at a relatively high value $kh = 1$.

Table 1. Error ΔU_1^h of the homogenized interface solution and error ΔU_2^h of the classical homogenization solution compared to the real solutions represented in the figures (Figures 4 and 5).

	Error ΔU_1^h	*Error* ΔU_2^h
$Q_m^{-1} = 0.05$, $Q_{in}^{-1} = 0.1$ and $e/h = 0.5$ (a-Fig.4)	0.4 %	0.6 %
$Q_m^{-1} = 0.2$, $Q_{in}^{-1} = 0.3$ and $e/h = 0.5$ (b-Fig.4)	0.5%	0.7%
$Q_m^{-1} = 0.1$, $Q_{in}^{-1} = 0.2$ and $e/h = 0.5$ (a-Fig.5)	0.5 %	0.7%
$Q_m^{-1} = 0.1$, $Q_{in}^{-1} = 0.2$ and $e/h = 1$ (b-Fig.5)	0.5%	0.7%

3.3.1. Transmission error as a function of frequencies

We first perform a validation for $Q_m^{-1} = 0.2$ and $Q_{in}^{-1} = 0.3$ (no Low loss media), for which we report the transmission spectra as a function of $K_R h \in [0.1]$ and $e/h \in [0.4]$, as well as the corresponding errors $\Delta T \equiv |T^{\text{num}} - T|/|T^{\text{num}}|$ (Figure 6).

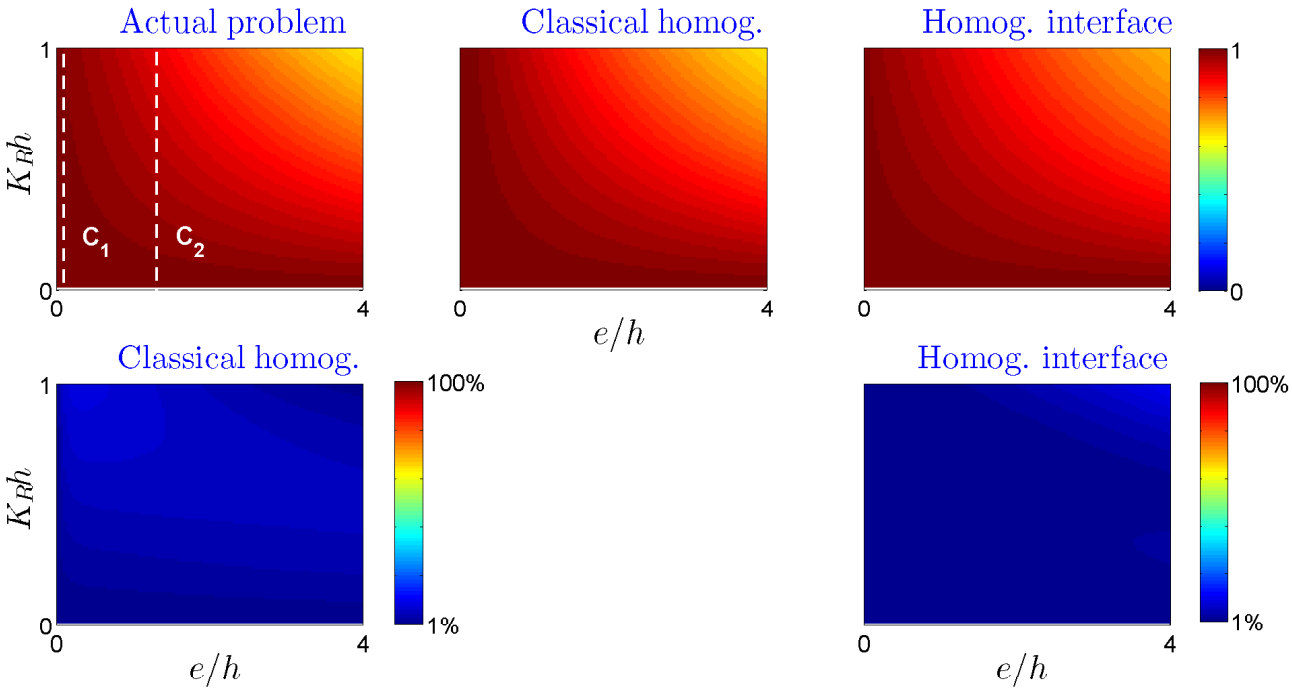

Fig. 6. Above: Transmission coefficients in the real $|T^{\text{num}}|$ and homogenized $|T|$ problem at the classical homogenization, and at the homogenized interface as a function of e/h and frequency $K_R h$; ($Q_m^{-1} = 0.2$, $Q_{in}^{-1} = 0.3$, $\varphi = 0.5$, $\theta = \pi/3$ and $\gamma = \pi/6$) were considered. Below: Errors ΔT on the transmission coefficient, which are calculated numerically. Errors less than 1% appear in dark blue, and errors greater than 100% appear in dark red.

In Figure 6 and for $Q_m^{-1} = 0.2$ and $Q_{in}^{-1} = 0.3$, the error in the transmission coefficient at the homogenized interface is less than 1% in the whole range of e/h, and it is 10% on average at classical homogenization. On the other hand, classical homogenization wrongly predicts the transmission coefficients for negligible thicknesses e/h, but by including the jump conditions (7) at the homogenized interface it restores the real scattering properties of a row of rectangular inclusions. This is consistent with the result of [34], in which the effective permittivity of electromagnetic waves must depend on thickness (the effective shear modulus parameter in our case).

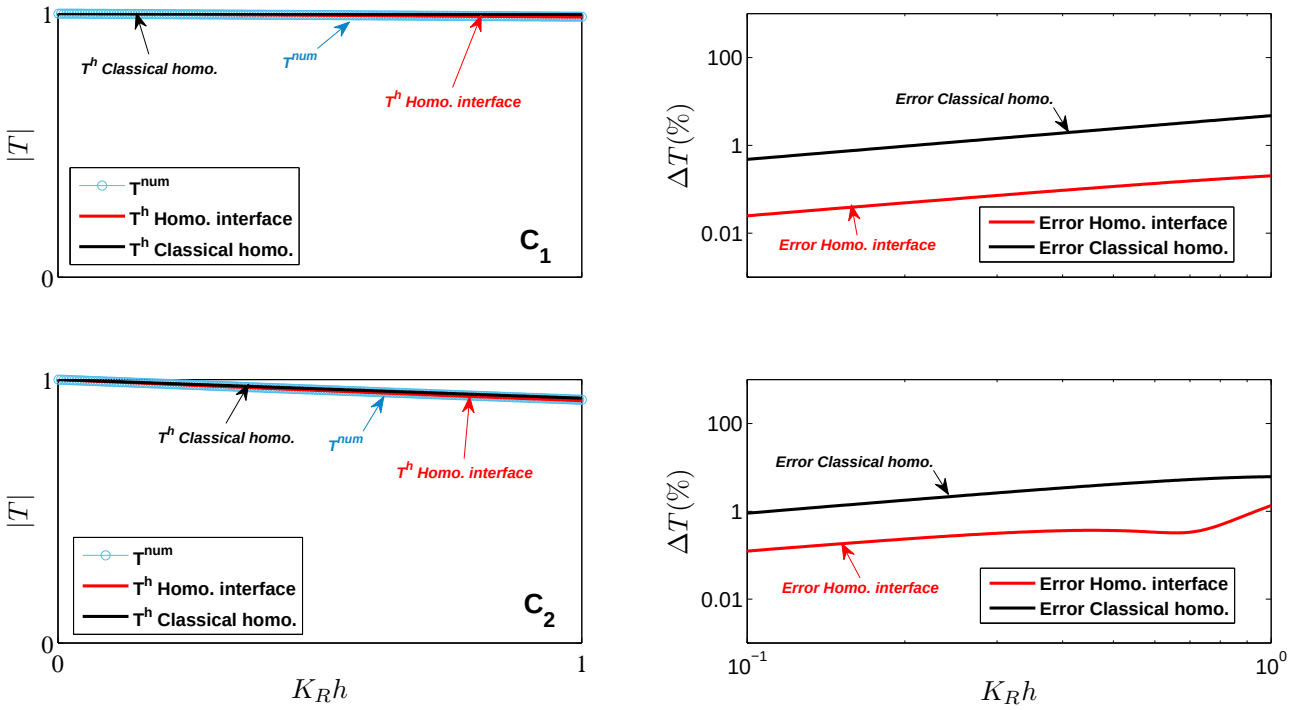

Fig. 7. Left: Transmission coefficients $|T^{\text{num}}|$ and $|T|$ as a function of $K_R h$ for $e/h = 0.05$ and $e/h = 1$ (C_1, C_2 profiles of Figure 6), with $|T^{\text{num}}|$: blue symbols and $|T|$: black lines the classic homogenization and red lines the homogenized interface. Right: The corresponding error ΔT of homogenized predictions, which are indicated as a percentage (black lines the classical homogenization and red lines the homogenized interface).

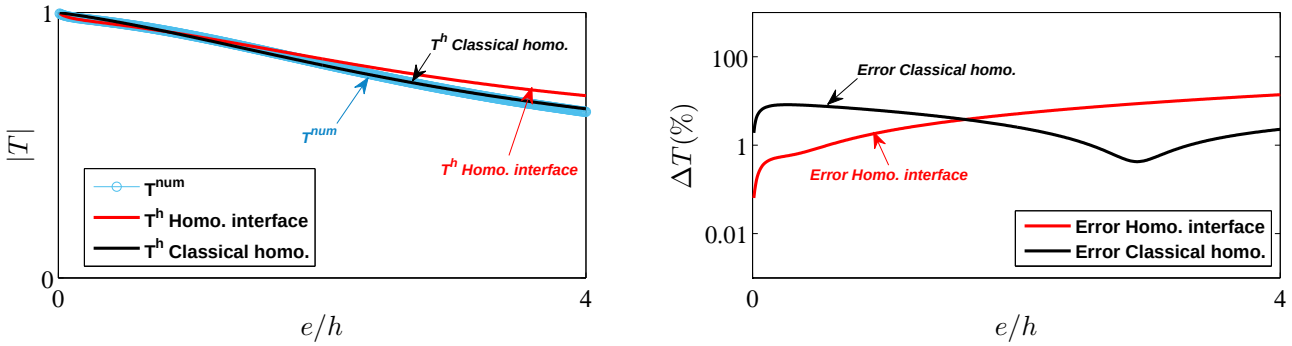

Fig. 8. Transmission coefficients $|T^{\text{num}}|$ and $|T|$ and errors ΔT as a function of e/h, for $K_R h = 1$. Same representation as in (Figure 7).

Specifically, we inspect (i) $|T^{\text{num}}|$ and its homogenized counterparts $|T|$, with the corresponding errors ΔT as a function of $K_R h$ for $e/h = 0.05$ and $e/h = 1$ (Figure 7). For a thin thickness (C_1 profile of Figure 6), the homogenized interface covers the actual transmission of the row of inclusions, while classical homogenization overestimates the transmission; for a row of thickness $e/h = 1$ (C_2 profile), the classical homogenization is valid for small values of $K_R h$; and applying the jump conditions allows us to increase the validity domain of the homogenized solution. (ii) Changes in $|T^{\text{num}}|$ and $|T|$ (and the corresponding errors ΔT) as a function of e/h for $K_R h = 1$ are reported in Figure 8. We notice that the grand error in classical homogenization seems to be a direct consequence of the disappearance of e/h.

3.3.2. Transmission error as a function of reciprocal quality factor

Finally, we show the variations of $|T^{\text{num}}|$ and its homogenized counterparts $|T|$, with the corresponding error ΔT based on Q_{in}^{-1} and Q_m^{-1} (Figure 9). In both cases and for $K_R h = 1$, the homogenized interface solution is valid by noting that the error of ΔT is less than 2% in the set of intervals of Q_{in}^{-1} or Q_m^{-1}.

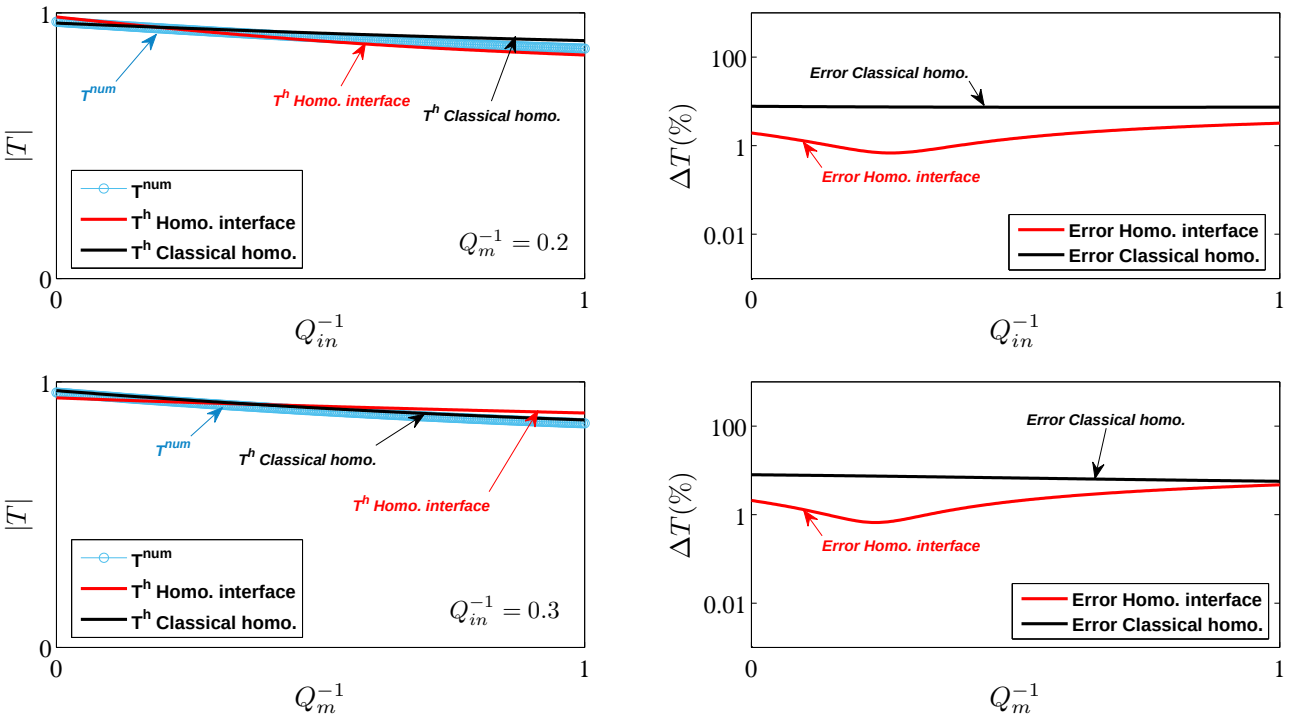

Fig. 9. Top: Transmission Coefficients $|T^{\text{num}}|$ (blue symbol), $|T|$ (black lines the classic homogenization and red lines the homogenized interface) and errors ΔT (black lines classical homogenization and red lines the homogenized interface) as a function of Q_{in}^{-1} for inclusions, with ($Q_m^{-1} = 0$, $K_R h = 1$, $e/h = 0.5$, $\varphi = 0.1$, $\theta = \pi/3$, $\gamma = \pi/6$). Bottom: Same representation as a function of Q_m^{-1} for the viscoelastic matrix, with $Q_{in}^{-1} = 0.3$.

4. Concluding remarks

In this article, we have presented a homogenized interface which can replace the physique problem of the scattering of shear waves at a periodic row of linear viscoelastic inclusions embedded in a linear viscoelastic matrix. Parameters effective of an equivalent interface enter in jump conditions for the displacement and the normal stress at the interface. They are obtained by the resolution of elementary problems written in the static limit, and they are therefore wave independent by construction. We have validated this model in the simple case of a rectangular inclusion and for a plane wave at oblique incidence on the row of linear viscoelastic inclusions. Note that this simplicity would be lost in the case of periodic media with a more complex unit cell. Finally, the explicit expressions of the transmission coefficients deduced from the effective interface parameters have been shown to be accurate for the Low–Loss viscoelastic media and no Low–Loss media, with a range of validity being $K_R h \leqslant 1$. On the other hand, classical homogenization wrongly predicts the transmission coefficients for negligible thicknesses e/h, but by including the jump conditions at the homogenized interface it restores the real scattering properties of a row of rectangular inclusions. The present model can be extended to a large class of wave problems, in acoustics and in electromagnetism.

Acknowledgments

The authors thank the anonymous reviewers for their insightful comments and suggestions.

Appendix A. Effective harmonic problem of a row of inclusions

Let us derive in this appendix the effective model. From the physical problems position (4), we noticed that the wave equation is identical to the one homogenized in [4,5,8–10,13,17–19,23,24,31,33], except that in our case, the coefficients of the physical parameters entering the wave equation are complex. Therefore, we obtained by analogy the same form of the homogenized wave equations at different orders.

We will apply the same asymptotic expansion technique as in [8] by dividing the space into two regions.

Fig. 10. Left: In the coordinate configuration x; the periodicity along x_2 is $\varepsilon \equiv K_R h$; the inner region is the neighborhood of the row of inclusions $-e/2 < (x_1 < e/2)$. Right: the unitary cell (inner region) in the coordinate y, with $\mathbf{y} = \mathbf{x}/\varepsilon$, and $\mathbf{y} \in \mathbb{R} \times Y$, with $Y = (-1/2, 1/2)$.

A.1. The matching asymptotic expansion

A.1.1. Inner and outer expansions

We consider the inner region ($|x_1| \ll 1$) and the outer region ($|x_1| \gg \varepsilon$), corresponding in terms of wave field to the near field and the far field, respectively (Figure 10). The outer regions are far enough from the row of inclusions that the evanescent field can be neglected. Then, the inner region and the outer regions are connected using so-called matching conditions, which will be the boundary conditions for the outer solutions. With this approach, the expansions read:

$$\begin{cases} \text{outer region, } |x_1| \gg \varepsilon, & u^\varepsilon = u^0(\mathbf{x}) + \varepsilon\, u^1(\mathbf{x}) + \dots, \\ & \sigma^\varepsilon = \sigma^0(\mathbf{x}) + \varepsilon\, \sigma^1(\mathbf{x}) + \dots, \\ \text{inner region, } |x_1| \ll 1, & u^\varepsilon = v^0(x_2, \mathbf{y}) + \varepsilon\, v^1(x_2, \mathbf{y}) + \dots, \\ & \sigma^\varepsilon = \tau^0(x_2, \mathbf{y}) + \varepsilon\, \tau^1(x_2, \mathbf{y}) + \dots, \end{cases} \tag{19}$$

with the outer terms (u^n, σ^n) for $x_1 < 0$ and the inner terms (v^n, τ^n) being Y periodic with $Y = (-1/2, 1/2)$; and now the second real problem (4) can be written in the inner and outer regions, thanks to the expansion of the following differential operator:

$$\begin{cases} \text{outer region,} & \nabla \to \nabla_{\mathbf{x}}, \\ \text{inner region,} & \nabla \to \dfrac{\partial}{\partial x_2} \mathrm{e}_2 + \dfrac{1}{\varepsilon} \nabla_{\mathbf{y}}, \end{cases} \tag{20}$$

where $\nabla_{\mathbf{x}}$ and $\nabla_{\mathbf{y}}$ means the gradient with respect to $\mathbf{x}$ and $\mathbf{y}$, as a macroscopic coordinate $\mathbf{x}$ associated with slow variations of the fields (with the particular scale $1/K_R$ of the wave) and a microscopic coordinate $\mathbf{y}$, associated with the fast variations (the particular h scale of the inclusions), and in the inner region, we keep the coordinates x_2 that are relevant to describe the variations of the field.

In the following, we will use the domain coordinate $\Omega = (-y_1^m, y_1^m) \times Y$ containing a single inclusion (Figure 10). Ω_i and Ω_m are the subdomains occupied respectively by the inclusion and by the matrix

($\Omega = \Omega_i \cup \Omega_m$); the continuities of the displacement and the normal stress apply on $\partial\Omega_i$. We will also use $\Omega_\infty = \lim_{y_1^m \to +\infty} \Omega$.

Finally, from (5), $(a^{*\varepsilon}, b^{*\varepsilon})$ can be specified in the outer regions ($|x_1| \gg \varepsilon$) as:

$$\begin{cases} a^{*\varepsilon}(\mathbf{x}) = 1, \\ b^{*\varepsilon}(\mathbf{x}) = \left(\dfrac{K^*}{K_R}\right)^2, \end{cases} \tag{21}$$

and in the inner region $a^{*\varepsilon}(\mathbf{x}) = \tilde{a}^*(\mathbf{x}/\varepsilon)$ and $b^{*\varepsilon}(\mathbf{x}) = \tilde{b}^*(\mathbf{x}/\varepsilon)$ with

$$\tilde{a}^*(\mathbf{y}) = \begin{cases} a^*(y_2), & \mathbf{y} \in \Omega_i, \\ 1, & \mathbf{y} \in \Omega_m, \end{cases} \qquad \tilde{b}^*(\mathbf{y}) = \begin{cases} b^*(y_2), & \mathbf{y} \in \Omega_i, \\ \left(\dfrac{K^*}{K_R}\right)^2, & \mathbf{y} \in \Omega_m, \end{cases} \tag{22}$$

with $a^*(y_2)$, $b^*(y_2)$ 1-periodic and piecewise complex constant.

A.1.2. Matching conditions

Because of the separation of the space into two regions, it is necessary to specify the boundary conditions at $|y_1| \to +\infty$ and for $x_1 \to 0^\pm$, which are unknown a priori. These conditions are provided by the matching conditions; they ensure the continuity of the displacement and the normal stress in an intermediate region where the evanescent field can be considered as negligible.

According to [35] the matching is written for $x_1 \to 0^\pm$ corresponding to $y_1 \to \pm\infty$. Due to the Taylor expansion of

$$\begin{aligned} u^0(x_1, x_2) &= u^0(0^\pm, x_2) + x_1 \partial_{x_1} u^0(0^\pm, x_2) + \dots \\ &= u^0(0^\pm, x_2) + \varepsilon y_1 \partial_{x_1} u^0(0^\pm, x_2) + \dots, \end{aligned}$$

even for σ^0; we obtain for $n = 0$:

$$\begin{cases} u^0(0^\pm, x_2) = \lim\limits_{y_1 \to \pm\infty} v^0(x_2, \mathbf{y}), & \text{(23a)} \\ \sigma^0(0^\pm, x_2) = \lim\limits_{y_1 \to \pm\infty} \tau^0(x_2, \mathbf{y}), & \text{(23b)} \end{cases}$$

and for $n = 1$:

$$\begin{cases} u^1(0^\pm, x_2) = \lim\limits_{y_1 \to \pm\infty} \left[v^1(x_2, \mathbf{y}) - y_1 \dfrac{\partial u^0}{\partial x_1}(0^\pm, x_2) \right], & \text{(24a)} \\ \sigma^1(0^\pm, x_2) = \lim\limits_{y_1 \to \pm\infty} \left[\tau^1(x_2, \mathbf{y}) - y_1 \dfrac{\partial \sigma^0}{\partial x_1}(0^\pm, x_2) \right]. & \text{(24b)} \end{cases}$$

A.2. Jump conditions and effective parameters

We start with the jump conditions $[\![v^0]\!]_0$ and $[\![\sigma_1^0]\!]_0$ at first order through an interface of zero thickness at $x_1 = 0$, with:

$$[\![f]\!]_0 \equiv f(0^+, x_2) - f(0^-, x_2). \tag{25}$$

A.2.1. Jump conditions at order 0

The real wave equations (4) for inner problem at first-order in ε^{-1} give:

$$\nabla_{\mathbf{y}} v^0 = 0, \quad \operatorname{div}_y \tau^0 = 0,$$

we deduce that v^0 does not depend on $\mathbf{y}$, so

$$u^0(0^-, x_2) = u^0(0^+, x_2) = v^0(x_2). \tag{26}$$

Then, integrating $\mathrm{div}_y \tau^0 = 0$ over $\mathbb{R} \times Y$ (Figure 11), and using (i) the continuity of $\tau^0 \cdot \mathbf{n}$ between inclusions along y_2, and (ii) the periodicity of τ^0 with respect to y_2, we obtain:

$$\int_Y \left[\tau_1^0(x_2, +\infty, y_2) - \tau_1^0(x_2, -\infty, y_2)\right] \mathrm{d}y_2 = 0.$$

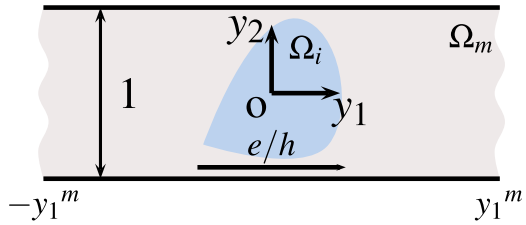

Fig. 11. The elementary cell in coordinates $\mathbf{y}$ with $\mathbf{y} \in \mathbb{R} \times Y$ ($Y = (-1/2, 1/2)$). In coordinates $\mathbf{y}$, we define $\Omega = (-y_1^m, y_1^m) \times Y$, with $y_1^m > e/h$ (In coordinates $\mathbf{y}$, we define $y_1^m \to +\infty$ will be taken into consideration); $\Omega = \Omega_\mathrm{i}$, with Ω_i and Ω_m the domains occupied by the inclusion and the matrix, respectively.

Finally, by integrating the matching conditions (23a) and (23b) on Y, we obtain

$$\int_Y \tau_1^0(x_2, \pm\infty, y_2)\, \mathrm{d}y_2 = \sigma_1^0(0^\pm, x_2). \tag{27}$$

Using (25), we deduce from (26)–(27) the jump conditions to the first order

$$[\![u^0]\!]_0 = [\![\sigma_1^0]\!]_0 = 0. \tag{28}$$

From (28), we find that the displacement and normal stress are continuous, which forces us to go to the next order to obtain the effect of the row of inclusions.

In order to obtain the second order jump conditions, we need to find the solutions of the elementary problems.

A.2.2. Jump conditions at order 1

Elementary problems and the jump condition on $\boldsymbol{u^1}$. From the first equation in (4) at order ε^{-1} and the second equation in (4) at order ε^0, the matching conditions (23b), it follows that the system satisfies by $v^1(x_2, \mathbf{y})$ can be written:

$$\begin{cases} \mathrm{div}_{\mathbf{y}}\, \tau^0 = 0 \quad \text{with} \quad \tau^0 = \tilde{a^*}(\mathbf{y}) \left[\dfrac{\partial u^0}{\partial x_2}(0, x_2)\mathbf{e}_2 + \nabla_{\mathbf{y}} v^1(x_2, \mathbf{y})\right], \\ v^1 \text{ and } \tau^0 \cdot \mathbf{n} \text{ continu on } \partial\Omega_i, \\ \lim\limits_{y_1 \to \pm\infty} \nabla_{\mathbf{y}} v^1(x_2, \mathbf{y}) = \dfrac{\partial u^0}{\partial x_1}(0, x_2)\mathbf{e}_1, \end{cases} \tag{29}$$

with v^1 and τ^0 periodic with respect to y_2. (29) is linear with respect to $\partial_{x_1} u^0(0, x_2)$ and $\partial_{x_2} u^0(0, x_2)$. Thus, we define $V^{(1)}(\mathbf{y})$ and $V^{(2)}(\mathbf{y})$ as

$$v^1(x_2, \mathbf{y}) = \frac{\partial u^0}{\partial x_1}(0, x_2) \left[V^{(1)}(\mathbf{y}) + y_1\right] + \frac{\partial u^0}{\partial x_2}(0, x_2) V^{(2)}(\mathbf{y}) + \hat{v}(x_2), \tag{30}$$

and for $i = 1, 2$,

$$\mathbf{T}^{(i)}(\mathbf{y}) \equiv \tilde{a^*}(\mathbf{y}) \nabla \left[V^{(i)}(\mathbf{y}) + y_i\right].$$

We see that the field v^1 in (29) is defined up to a function of x_2, and it is denoted $\hat{v}(x_2)$ in (30); we will see that the determination of $\hat{v}(x_2)$ is not necessary. It is easy to see that if $(V^{(i)}, \mathbf{T}^{(i)})$ satisfy the elementary problems:

$$\begin{cases} \mathrm{div}\, \mathbf{T}^{(i)} = 0 \quad \text{with} \quad \mathbf{T}^{(i)}(\mathbf{y}) \equiv \tilde{a}^*(\mathbf{y}) \nabla \left[V^{(i)}(\mathbf{y}) + y_i\right], \\ V^{(i)} \text{ and } \mathbf{T}^{(i)} \cdot \mathbf{n} \text{ continuous on } \partial\Omega_i, \\ \lim\limits_{y_1 \to \pm\infty} \nabla V^{(i)}(\mathbf{y}) = 0. \end{cases} \tag{31}$$

then $v^1(x_2, \mathbf{y})$ satisfied (29).

From (31), $V^{(i)}$ for $i = 1, 2$, being defined up to a constant, can be chosen as:

$$V^{(i)}(\mathbf{y}) = \begin{cases} V_{ev}^{(i)}(\mathbf{y}), & y_1 < 0, \\ \mathcal{B}_i + V_{ev}^{(i)}(\mathbf{y}), & y_1 > 0, \end{cases}$$

where $V_{ev}^{(i)}(\mathbf{y})$, $i = 1, 2$ are evanescent fields, vanishing at $y_1 \to \pm\infty$. Thus,

$$\mathcal{B}_i \equiv V^{(\mathrm{i})}(+\infty, y_2) - V^{(\mathrm{i})}(-\infty, y_2) \tag{32}$$

with $\mathcal{B}_i$ being constant values ($i = 1, 2$), and are called the first interface parameters. It is now enough to use the matching condition (24a) to obtain:

$$[\![u^1]\!]_0 = \mathcal{B}_1 \frac{\partial u^0}{\partial x_1}(0, x_2) + \mathcal{B}_2 \frac{\partial u^0}{\partial x_2}(0, x_2), \tag{33}$$

which provides the first jump condition written here for u^1 across an interface of zero thickness at $x_1 = 0$.

The jump condition on $\boldsymbol{\sigma_1^1}$. The derivation of the jump condition on ${\sigma_1}^1$ is more demanding and requires integrating more than Ω the first equation of (4) to order ε^0 for the inner solution, which reads as follows:

$$v^0(0, x_2) \int_\Omega \tilde{b}^*(\mathbf{y})\, \mathrm{d}\mathbf{y} + \int_\Omega \left[\mathrm{div}_{\mathbf{y}}\, \tau^1 + \frac{d\tau_2^0}{\partial x_2} \right] \mathrm{d}\mathbf{y} = 0, \tag{34}$$

where we used (26). After doing this, we inspect the τ_2^0 term that is needed in the above equation. From (31) and (30), we have:

$${\tau_2}^0 = \tilde{a^*}(\mathbf{y}) \left[\frac{\partial u^0}{\partial x_1}(0, x_2) \frac{\partial V^{(1)}}{\partial y_2} + \frac{\partial u^0}{\partial x_2}(0, x_2) \left(\frac{\partial V^{(2)}}{\partial y_2} + 1 \right) \right].$$

It is now enough to use the second equation of (4) for the problem outside the order ε^0 to obtain:

$${\sigma_1}^0 = \frac{\partial u^0}{\partial x_1}, \quad {\sigma_2}^0 = \frac{\partial u^0}{\partial x_2},$$

and therefore:

$$\tau_2^0 = \tilde{a}^*(\mathbf{y}) \left[\sigma_1^0(0, x_2) \frac{\partial V^{(1)}}{\partial y_2} + \sigma_2^0(0, x_2) \left(\frac{\partial V^{(2)}}{\partial y_2} + 1 \right) \right]. \tag{35}$$

We can return to the equation (34), which involves three integrals. The first integral is:

$$u^0(0, x_2) \int_\Omega \tilde{b}^*(\mathbf{y})\, \mathrm{d}\mathbf{y} = \left(\frac{K^*}{K_R} \right)^2 u^0(0, x_2) \left[2y_1^m + \frac{e\varphi}{h} \left(\frac{\rho_i}{\rho_m} - 1 \right) \right], \tag{36}$$

with $e\varphi/h$ the surface of the inclusion in coordinates y (φ is the filling fraction of the inclusion for $y_1 \in (0, e/h)$) (Figure 11). The second integral, of $\mathrm{div}_{\mathbf{y}}$, is obtained thanks to the continuity of $\tau^1 \cdot \mathbf{n}$ and its periodicity with respect to y_2, and we obtain

$$\int_\Omega \mathrm{div}_{\mathbf{y}} \tau_1\, \mathrm{d}\mathbf{y} = \int_Y \left[\tau_1^1(+y_1^m, y_2, x_2) - \tau_1^1(-y_1^m, y_2, x_2) \right] \mathrm{d}y_2 \tag{37}$$

for the third integral, with $\partial_{x_2} \tau_2^0$ given by (35), we have

$$\begin{aligned} \int_\Omega \frac{\partial \tau_2^0}{\partial x_2}\, \mathrm{d}\mathbf{y} = {} & \frac{\partial \sigma_1^0}{\partial x_2}(0, x_2) \int_\Omega \tilde{a}^*(\mathbf{y}) \frac{\partial V^{(1)}}{\partial y_2} \\ & \frac{\partial \sigma_2^0}{\partial x_2}(0, x_2) \left[\int_\Omega \tilde{a}^*(\mathbf{y}) \frac{\partial V^{(2)}}{\partial y_2} + 2y_1^m + \frac{e\varphi}{h} \left(\frac{M_i}{M_m} - 1 \right) \right]. \end{aligned} \tag{38}$$

Two terms in (36) and in (38), are linear in y_1^m. They are added together to obtain:

$$2y_1^m \left[\left(\frac{K^*}{K_R} \right)^2 u^0(0, x_2) + \frac{\partial \sigma_2^0}{\partial x_2}(0, x_2) \right] = -2y_1^m \frac{\partial \sigma_1^0}{\partial x_1}(0, x_2), \tag{39}$$

where we used the second equation of (4) for the inner problem of order ε^0, in particular:

$$\frac{\partial \sigma_1^0}{\partial x_1} + \frac{\partial \sigma_2^0}{\partial x_2} + \left(\frac{K^*}{K_R} \right)^2 u^0 = 0. \tag{40}$$

We now add two terms of (37) and (39) using the matching conditions (24b) written in another form:

$$\begin{cases} \sigma_1^1(0^-,x_2) = \lim\limits_{y_1^m\to+\infty}\left[\tau_1^1(-y_1^m,y_2,x_2) + y_1^{\mathrm{m}}\dfrac{\partial\sigma_1^0}{\partial x_1}(0^-,x_2)\right], \\ \sigma_1^1(0^+,x_2) = \lim\limits_{y_1^m\to+\infty}\left[\tau_1^1(y_1^m,y_2,x_2) - y_1^{\mathrm{m}}\dfrac{\partial\sigma_1^0}{\partial x_1}(0^+,x_2)\right], \end{cases} \tag{41}$$

and because of the continuity of σ_1^0 at $y_1=0$, we get

$$[\![\sigma_1^1]\!]_0 = \lim_{y_1^m\to\infty}\left[\tau_1^1(y_1^m,y_2,x_2) - \tau_1^1(-y_1^{\mathrm{m}},y_2,x_2) - 2y_1^{\mathrm{m}}\frac{\partial\sigma_1^0}{\partial x_1}(0,x_2)\right],$$

including equations (36) to (39) in (34) for $y_1^m\to+\infty$, and using the above equation, we get:

$$\begin{aligned}[\![\sigma_1^1]\!]_0 = &-\left(\frac{K^*}{K_R}\right)^2 u^0(0,x_2)\frac{e\varphi}{h}\left(\frac{\rho_i}{\rho_m}-1\right) - \frac{\partial\sigma_1^0}{\partial x_2}(0,x_2)\int_{\Omega_\infty}\tilde{a}^*(\mathbf{y})\frac{\partial V^{(1)}}{\partial y_2} \\ &- \frac{\partial\sigma_2^0}{\partial x_2}(0,x_2)\left[\int_{\Omega_\infty}\tilde{a}^*(\mathbf{y})\frac{\partial V^{(2)}}{\partial y_2} + \frac{e\varphi}{h}\left(\frac{M_i}{M_m}-1\right)\right].\end{aligned}$$

Finally, with (40), the jump of σ_1^1 through an interface of zero thickness at $x_1=0$ is written:

$$[\![\sigma_1^1]\!]_0 = \frac{e\varphi}{h}\left(\frac{\rho_i}{\rho_m}-1\right)\frac{\partial\sigma_1^0}{\partial x_1}(0,x_2) - \mathcal{C}_1\frac{\partial\sigma_1^0}{\partial x_2}(0,x_2) - \left[\mathcal{C}_2 + \frac{e\varphi}{h}\left(\frac{M_i}{M_m}-\frac{\rho_i}{\rho_m}\right)\right]\frac{\partial\sigma_2^0}{\partial x_2}(0,x_2), \tag{42}$$

where we have defined the parameters of the second interface, for $i=1,2$,

$$\mathcal{C}_i \equiv \int_{\Omega_\infty}\tilde{a}^*(\mathbf{y})\frac{\partial V^{(\mathrm{i})}}{\partial y_2}\,\mathrm{d}\mathbf{y}. \tag{43}$$

A.3. The homogenized problem and the associated final jump conditions

The final jump conditions will be written, from (33) and (42), in a different form and equivalent up to $O(\varepsilon^2)$ to those obtained for $u^0+\varepsilon u^1$ and for $\sigma_1^0+\varepsilon\sigma_1^1$. From (4), u and σ_1 up to $O(\varepsilon^2)$ satisfies the Helmholtz equation in the matrix and jump conditions through a zero thickness interface at $x_1=0$, which reads as follows:

$$\begin{cases} \Delta u + u = 0, \\ [\![u]\!]_0 = \varepsilon\,\mathcal{B}_1\dfrac{\partial u^0}{\partial x_1}(0,x_2) + \varepsilon\,\mathcal{B}_2\dfrac{\partial u^0}{\partial x_2}(0,x_2) + O(\varepsilon^2), \\ [\![\sigma_1]\!]_0 = \varepsilon\dfrac{e\varphi}{h}\left(\dfrac{\rho_i}{\rho_m}-1\right)\dfrac{\partial\sigma_1^0}{\partial x_1}(0,x_2) - \varepsilon\,\mathcal{C}_1\dfrac{\partial\sigma_1^0}{\partial x_2}(0,x_2) \\ \qquad\qquad - \varepsilon\left[\mathcal{C}_2 + \dfrac{e\varphi}{h}\left(\dfrac{M_i}{M_m}-\dfrac{\rho_i}{\rho_m}\right)\right]\dfrac{\partial\sigma_2^0}{\partial x_2}(0,x_2) + O(\varepsilon^2). \end{cases} \tag{44}$$

It has been shown in [4,5,11,36] that it is better to express the jump conditions through an extended version of the interface. First, we define an enlarged version of the jumps and associated mean value for any field $f(x_1,x_2)$,

$$[\![f]\!] \equiv f^+ - f^-, \quad \bar{f} \equiv \frac{1}{2}\left[f^- + f^+\right], \quad \text{with} \quad f^\pm = f\left(\pm\frac{eK_R}{2},x_2\right).$$

We now use the Taylor expansion

$$u^0\left(\pm\frac{eK_R}{2},x_2\right) = u^0\left(0^\pm,x_2\right) \pm \varepsilon\frac{e}{2h}\frac{\partial u^0}{\partial x_1}\left(\pm\frac{eK_R}{2},x_2\right) + O(\varepsilon^2),$$

where we used $e/h=O(1)$, and with (44), we obtain the jump condition:

$$[\![u]\!] = \varepsilon\left(B_1+\frac{e}{h}\right)\overline{\frac{\partial u}{\partial x_1}} + \varepsilon B_2\overline{\frac{\partial u}{\partial x_2}} + O(\varepsilon^2),$$

(and the same thing to get the jump from $[\![\sigma_1]\!]$). Now, after [7], we define the new homogenized problem in rescaled coordinates:

$$\begin{cases} \Delta u^h + u^h = 0, \\ [\![u^h]\!] = \varepsilon \mathcal{B} \overline{\dfrac{\partial u^h}{\partial x_1}} + \varepsilon B_2 \overline{\dfrac{\partial u^h}{\partial x_2}}, \\ [\![\sigma_1^h]\!] = \varepsilon \left[\mathcal{S} \overline{\operatorname{div} \sigma^h} - \mathcal{C}_1 \overline{\dfrac{\partial {\sigma_1}^h}{\partial x_2}} - \mathcal{C} \overline{\dfrac{\partial {\sigma_2}^h}{\partial x_2}} \right], \end{cases} \tag{45}$$

with

$$\mathcal{B} \equiv \frac{e}{h} + \mathcal{B}_1, \quad \mathcal{C} \equiv \frac{e}{h} + \frac{e\varphi}{h} \left(\frac{M_i}{M_m} - 1 \right) + \mathcal{C}_2, \quad S \equiv \frac{e}{h} + \frac{e\varphi}{h} \left(\frac{\rho_i}{\rho_m} - 1 \right).$$

It is easy to see that $\left(v^h, \sigma^h\right)$ has the same expansions as (v, σ) up to $O(\varepsilon^2)$.

[1] Hubert J. S., Sanchez-Hubert J. Introduction aux Méthodes Asymptotiques et à l'homogénéisation: Application à La Mécanique Des Milieux Continus. Masson (1992).

[2] Bensoussan A., Lions J.-L., Papanicolaou G. Asymptotic Analysis for Periodic Structures. American Mathematical Society (2011).

[3] Lapine M., McPhedran R. C., Poulton C. G. Slow Convergence to Effective Medium in Finite Discrete Metamaterials. Physical Review B. **93** (23), 235156 (2016).

[4] Marigo J.-J., Maurel A. Homogenization Models for Thin Rigid Structured Surfaces and Films. The Journal of the Acoustical Society of America. **140** (1), 260–273 (2016).

[5] Marigo J.-J., Maurel A. An Interface Model for Homogenization of Acoustic Metafilms. World Scientific Series in Nanoscience and Nanotechnology, World Scientific Handbook of Metamaterials and Plasmonics. 599–645 (2017).

[6] Marigo J.-J., Pideri C. The Effective Behavior of Elastic Bodies Containing Microcracks or Microholes Localized on a Surface. International Journal of Damage Mechanics. **20** (8), 1151 (2011).

[7] David M., Marigo J.-J., Pideri C. Homogenized Interface Model Describing Inhomogeneities Located on a Surface. Journal of Elasticity. **109** (2), 153–187 (2012).

[8] Marigo J.-J., Maurel A., Pham K., Sbitti A. Effective Dynamic Properties of a Row of Elastic Inclusions: The Case of Scalar Shear Waves. Journal of Elasticity. **128** (2), 265–289 (2017).

[9] Pham K., Maurel A., Marigo J.-J. Revisiting Imperfect Interface Laws for Two-Dimensional Elastodynamics. Proceedings of the Royal Society A: Mathematical, Physical and Engineering Sciences. **477** (2245), 20200519 (2021).

[10] Pham K., Maurel A., Marigo J.-J. Two scale homogenization of a row of locally resonant inclusions — the case of anti-plane shear waves. Journal of the Mechanics and Physics of Solids. **106**, 80–94 (2017).

[11] Delourme B., Haddar H., Joly P. Approximate models for wave propagation across thin periodic interfaces. Journal de Mathématiques Pures et Appliquées. **98** (1), 28–71 (2012).

[12] Delourme B., Haddar H., Joly P. On the Well-Posedness, Stability and Accuracy of an Asymptotic Model for Thin Periodic Interfaces in Electromagnetic Scattering Problems. Mathematical Models and Methods in Applied Sciences. **23** (13), 2433–2464 (2013).

[13] Ourir A., Gao Y., Maurel A., Marigo J.-J. Homogenization of Thin and Thick Metamaterials and Applications. Borja, Alejandro Lucas, InTech (2017).

[14] Bonnet-Bendhia A. S., Drissi D., Gmati N. Simulation of Muffler's Transmission Losses by a Homogenized Finite Element Method. Journal of Computational Acoustics. **12** (03), 447–474 (2004).

[15] Belemou R., Sbitti A., Marigo J.-J., Tsouli A. Homogenization of subwavelength free stratified edge of viscoelastic media including finite size effect. Mathematical Modeling and Computing. **10** (1), 10–29 (2023).

[16] Belemou R., Sbitti A., Marigo J.-J., El Amri H. Homogenization of the Helmholtz Problem with Layered Viscoelastic Media Including Finite Size Effect. IAENG International Journal of Applied Mathematics. **53** (1), 282–293 (2023).

[17] Marigo J.-J., Maurel A. Second Order Homogenization of Subwavelength Stratified Media Including Finite Size Effect. SIAM Journal on Applied Mathematics. **77** (2), 721–743 (2017).

[18] Marigo J.-J., Maurel A. Two-Scale Homogenization to Determine Effective Parameters of Thin Metallic–Structured Films. Proceedings of the Royal Society A: Mathematical, Physical and Engineering Sciences. **472** (2192), 20160068 (2016).

[19] Maurel A., Marigo J.-J., Ourir A. Homogenization of ultrathin metallo-dielectric structures leading to transmission conditions at an equivalent interface. Journal of the Optical Society of America B. **33** (5), 947–956 (2016).

[20] Abdelmoula R., Coutris M., Marigo J.-J. Comportement asymptotique d'une interphase élastique mince. Comptes Rendus de l'Académie des Sciences – Series IIB – Mechanics-Physics-Chemistry-Astronomy. **326** (4), 237–242 (1998).

[21] Rizzoni R., Dumont S., Lebon F., Sacco E. Higher order model for soft and hard elastic interfaces. International Journal of Solids and Structures. **51** (23–24), 4137–4148 (2014).

[22] Rizzoni R., Dumont S., Lebon F. On Saint Venant–Kirchhoff Imperfect Interfaces. International Journal of Non-Linear Mechanics. **89**, 101–115 (2017).

[23] Mercier J.-F., Marigo J.-J., Maurel A. Influence of the neck shape for Helmholtz resonators. The Journal of the Acoustical Society of America. **142** (6), 3703–3714 (2017).

[24] Maurel A., Marigo J.-J., Mercier J.-F., Pham K. Modelling resonant arrays of the Helmholtz type in the time domain. Proceedings of the Royal Society A: Mathematical, Physical and Engineering Sciences. **474** (2210), 20170894 (2018).

[25] Lebon F., Rizzoni R. Asymptotic Behavior of a Hard Thin Linear Elastic Interphase: An Energy Approach. International Journal of Solids and Structures. **48** (3), 441–449 (2011).

[26] Dumont S., Rizzoni R., Lebon F., Sacco E. Soft and hard interface models for bonded elements. Composites Part B: Engineering. **153**, 480–490 (2018).

[27] Lebon F., Rizzoni R. Higher Order Interfacial Effects for Elastic Waves in One Dimensional Phononic Crystals via the Lagrange–Hamilton's Principle. European Journal of Mechanics – A/Solids. **67**, 58–70 (2018).

[28] Capdeville Y., Marigo J.-J. A Non-periodic two scale asymptotic method to take account of rough topographies for 2-D elastic wave propagation. Geophysical Journal International. **192** (1), 163–189 (2013).

[29] Cioranescu D., Donato P. An Introduction to Homogenization. Oxford Lecture Series in Mathematics and Its Applications. Vol. 17, Oxford University Press, Oxford, New York (1999).

[30] Borcherdt R. D. Viscoelastic Waves in Layered Media. Cambridge University Press, Cambridge (2009).

[31] Pham K., Maurel A., Mercier J.-F., Félix S., Cordero M. L., Horvath C. Perfect Brewster transmission through ultrathin perforated films. Wave Motion. **93**, 102485 (2020).

[32] Gumerov N., Duraiswami R. Fast Multipole Methods for the Helmholtz Equation in Three Dimensions. Elsevier (2004).

[33] Petit R. Electromagnetic Theory of Gratings. Topics in Current Physics. Springer-Verlag, Berlin, Heidelberg (1980).

[34] Lalanne P., Lemercier-Lalanne D. Depth dependence of the effective properties of subwavelength gratings. Journal of the Optical Society of America A. **14** (2), 450–459 (1997).

[35] Abdelmoula R. The effective behavior of a fiber bridged crack. Journal of the Mechanics and Physics of Solids. **48** (11), 2419–2444 (2000).

[36] Delourme B. High-order asymptotics for the electromagnetic scattering by thin periodic layers. Mathematical Methods in the Applied Sciences. **38** (5), 811–833 (2015).

Гомогенізація задачі Гельмгольца за наявності ряду в'язкопружних включень

Белемоу Р.[1], Сбітті А.[2], Джауахрі М.[1], Маріго Ж.-Ж.[3]

[1] *Університет Хасана II, Енс,*
вул. Ель Джадіда Км 9, Ганді, 50069, Касабланка, Марокко
[2] *Університет Мохаммеда V, Енсам,*
вул. Об'єднаних Націй, Агдал, 8007.N.U, Рабат, Марокко
[3] *Лабораторія механіки твердого тіла, Політехнічна школа,*
91128, Палезо, Франція

Запропоновано метод гомогенізації, який заснований на техніці узгодженого асимптотичного розвинення, щоб отримати ефективну поведінку періодичного масиву лінійних в'язкопружних включень, які вбудовані у лінійну в'язкопружну матрицю. Розглянуто задачу для зсувних хвиль і хвильове рівняння в гармонічному режимі. Отримана ефективна поведінка відповідає еквівалентній межі поділу, яка пов'язана з умовами стрибка, для зміщення та нормального напруження на межі поділу. Коефіцієнти пропускання та поля зміщень отримані в замкнених формах і перевірена їх справедливість шляхом порівняння з числовими результатами у випадку прямокутних включень.

Ключові слова: *гомогенізація; узгоджене асимптотичне розкладання; субхвильова шкала; передача хвиль; в'язкопружний; гомогенізація межі поділу; ефективні умови стрибка.*